Earth and Space Science

RESEARCH ARTICLE
10.1029/2020EA001427

IASI-Derived Sea Surface Temperature Data Set for Climate Studies

Ana C. Parracho[1], Sarah Safieddine[1], Olivier Lezeaux[2], Lieven Clarisse[3], Simon Whitburn[3], Maya George[1], Pascal Prunet[2], and Cathy Clerbaux[1,3]

[1]LATMOS/IPSL, UVSQ, CNRS, Sorbonne Université, Paris, France, [2]SPASCIA, Toulouse, France, [3]Spectroscopy, Quantum Chemistry and Atmospheric Remote Sensing (SQUARES), Université Libre de Bruxelles (ULB), Brussels, Belgium

Key Points:

- First IASI algorithm focused on sea surface temperature (SST) suitable for climate studies
- The IASI-derived SST data set is compared with other available data sets
- Climate variability and trends are shown and compared to other data sets

Supporting Information:

Supporting Information may be found in the online version of this article.

Correspondence to:

A. C. Parracho,
ana-claudia.parracho@latmos.ipsl.fr

Citation:

Parracho, A. C., Safieddine, S., Lezeaux, O., Clarisse, L., Whitburn, S., George, M., et al. (2021). IASI-derived sea surface temperature data set for climate studies. *Earth and Space Science*, *8*, e2020EA001427. https://doi.org/10.1029/2020EA001427

Received 2 SEP 2020
Accepted 22 MAR 2021

Abstract

Sea surface temperature (SST) is an essential climate variable, that is directly used in climate monitoring. Although satellite measurements can offer continuous global coverage, obtaining a long-term homogeneous satellite-derived SST data set suitable for climate studies based on a single instrument is still a challenge. In this work, we assess a homogeneous SST data set derived from reprocessed Infrared Atmospheric Sounding Interferometer (IASI) level-1 (L1C) radiance data. The SST is computed using Planck's Law and simple atmospheric corrections. We assess the data set using the ERA5 reanalysis and the EUMETSAT-released IASI level-2 SST product. Over the entire period, the reprocessed IASI SST shows a mean global difference with ERA5 close to zero, a mean absolute bias under 0.5°C, with a SD of difference around 0.3°C and a correlation coefficient over 0.99. In addition, the reprocessed data set shows a stable bias and SD, which is an advantage for climate studies. The interannual variability and trends were compared with other SST data sets: ERA5, Hadley Centre's SST (HadISST), and NOAA's Optimal Interpolation SST Analysis (OISSTv2). We found that the reprocessed SST data set is able to capture the patterns of interannual variability well, showing the same areas of high interannual variability (>1.5°C), including over the tropical Pacific in January corresponding to the El Niño Southern Oscillation. Although the period studied is relatively short, we demonstrate that the IASI data set reproduces the same trend patterns found in the other data sets (i.e., cooling trend in the North Atlantic, warming trend over the Mediterranean).

Plain Language Summary

Sea surface temperature (SST) is an essential variable for monitoring climate, as defined by the Global Climate Observing System (GCOS; https://gcos.wmo.int/en/essential-climate-variables/sst). Satellite measurements can offer global continuous SST measurements, but their stability over the time needs to be assured. In this work, we present a new data set derived from the Infrared Atmospheric Sounding Interferometer, IASI (flying aboard the Metop satellites), and compare it with other available data sets. This comparison shows that our data set produces similar means, variability and trends as other data sets, with the advantage that it is derived with a single algorithm from a single well-calibrated instrument. This assures there are no substantial changes to the instrument characteristics over time that might result in artificial trends.

1. Introduction

Sea surface temperature (SST) is an essential climate variable (ECV) as defined by the global climate observing system (GCOS), that is used directly in the monitoring of climate trends and variability, or as boundary conditions in climate models (e.g., Robinson et al., 2012). The implications of SST data in climate analysis and modeling has been studied extensively (e.g., Hurrell & Trenberth, 1999; Rayner, Kaplan, et al., 2009).

SST is relatively easy to observe, and has a long observational history (well documented in Barton 1995; Bottomley et al., 1990; Emery, Castro, et al., 2001; Minnett, Alvera-Azcárate, et al., 2019). Data records of SST started with in situ measurement by moving sailing vessels and ships, and later with satellite-tracked and satellite-reporting moored and drifting buoys. These measurements, taken from a few tens of centimeters of water to up to 5 m below the sea surface, are known as the sub-skin SST. From the mid1970s, SSTs started also being computed from infrared satellite data. Satellite radiances are converted into skin SST, which corresponds to the SST measured at about 10 μm below the surface of the sea (Emery, Castro, et al., 2001). This

is the temperature of the molecular boundary between air and sea, where the transfer of heat, momentum, and gases (such as CO_2) occurs. Sub-skin and skin SSTs are different. Emery, Castro, et al. (2001) have determined their mean differences to be around 0.3°C and instantaneous differences to vary as a function of air-sea heat fluxes and the wind speed at the surface. These differences can range from negligible (at nighttime, under windy conditions, when there is low insolation and high vertical mixing) to several degrees (when there is high insolation and sustained low wind speeds) (Merchant, 2013). Donlon, Minnett, et al. (2002) have found skin SST to be around 0.17°C cooler than sub-skin SST when free of diurnal warming effects, and at wind-speeds greater than 6 m/s. Although the skin effect is a different physical effect from the diurnal variation, when diurnal variations are large, the skin effect can be confused (especially when there is low wind speed and higher insolation). Satellite and in situ measurements are complementary to each other and are often blended in one data set (e.g., National Oceanic and Atmospheric Administration [NOAA] Optimum Interpolation Sea Surface temperature [OISST]), where the sub-skin/skin SST differences are taken into account. Infrared satellites always measure skin SST, however, some products are adjusted to report a sub-skin SST, dependent on the users. Monitoring of the SST derived from satellites is promoted by the group for high resolution sea surface temperature (GHRSST; www.ghrsst.org), which provides a framework for SST data sharing, best practices for data processing.

Satellite measurements offer a global horizontal coverage, and a continuous synoptic temporal coverage, which allows for a more uniform coverage than in situ measurements (Lee & Gentemann, 2018). As such, satellite measurements resolve features that are not captured by in situ measurements, such as large-scale signals and teleconnections (e.g., El Niño/Southern Oscillation [ENSO]), and small-scale features such as fronts and eddies. In addition, they also cover areas of difficult access, such as the high latitude oceans, where in situ measurements are scarce. Because of these advantages, operational satellite-derived SSTs are used to support weather forecasting and near real-time oceanography. Satellite SST retrievals are available from a variety of polar-orbiting and geostationary platforms carrying microwave and infrared sensors (Robinson & Donlon, 2003). These include the Spinning Enhanced Visible and Infrared Imager (SEVIRI) onboard the geostationary Meteosat Second Generation (e.g., Robinson et al., 2012), the Advanced Very High Resolution Radiometer (AVHRR) sensors onboard the different NOAA polar orbiting platforms (e.g., Casey et al., 2010) and more recently on the suite of Metop satellites (e.g., Le Borgne et al., 2007; Marsouin et al., 2015), the Moderate Resolution Imaging Spectroradiometer (MODIS) on board of the Terra and Aqua satellites (Minnett, Evans, et al., 2002), the Atmospheric InfraRed Sounder (AIRS, Aumann et al., 2003), aboard the Aqua satellite, and from the Infrared Atmospheric Sounding Interferometer (IASI) on board the three Metop satellites since 2007, 2012, and 2018 (August et al., 2012; O'Carroll et al., 2012; Siméoni et al., 1997). More recently, SST is also measured by the sea and land surface temperature radiometer (SLSTR) as part of the European Sentinel Mission, Sentinel-3 (Donlon, Berruti, et al., 2012). As part of the European Space Agency Climate Change Initiative Sea Surface Temperature project (ESA SST CCI), a consistent re-analysis of daily 0.05° × 0.05° resolution SSTs from 1981 to 2016 has been produced using observations from both the AVHRR and along track scanning radiometer (ATSR) and a data assimilation method where there were no measurements (Good et al., 2019; Merchant, Embury, et al., 2019).

IASI onboard Metop has a polar orbit that covers the entire Earth's surface twice a day, in the morning and evening. The instrument was designed for numerical weather prediction and atmospheric composition monitoring (Clerbaux, Boynard, et al., 2009; Collard et al., 2009; Hilton et al., 2012), but with more than 13 years of readily available data to date, with the prospect of having a similar instrument until 2040 with the IASI-NG mission, IASI can also be used in climate research. Although interest in exploiting spectrally resolved data to study climate variability has been previously highlighted (Brindley et al., 2015; Clerbaux, Hadji-Lazaro, et al., 2003; Smith et al., 2015), and the need to construct a climate data record is becoming increasingly evident, relatively little has been done so far to generate consistent records for climate variables with IASI (i.e., derived with a single algorithm from a single well-calibrated instrument, with no substantial changes to the instrument characteristics over time). In order to be adequate for use in climate applications, SST data must be not only accurate, but also consistent over time (i.e., homogeneous). Since IASI is a long-term "sentinel" mission that is planned for flying at least 18 years, with the three instruments built at the same time and flying in constellation, continuity and stability of IASI-derived data are ensured. In fact, due to its stability, IASI is used as the reference instrument in the Global Space-based Inter-Calibration System (GSICS) (Hewison et al., 2013). Finally, long-term continuation of the program is also guaranteed,

as the new generation of Infrared Atmospheric Sounding Interferometers (IASI-NG) (Clerbaux & Crevoisier, 2013; Crevoisier et al., 2014), will be launched on three successive Metop—Second Generation satellites within the 2023–2040 timeframe.

Although there is an operational IASI SST product available from EUMETSAT (L2Pcore) that is complemented by the EUMETSAT OSI SAF IASI SST product (GHRSST L2P), the goal of this study is to obtain a long-term IASI (only)-derived SST data set and assess if it is suitable for climate studies (trend estimation and interannual variability in particular). This data set, as compared to other data sets will have the advantage of being global (as opposed to geostationary satellites), homogeneous, and uniform (uses one instrument); an essential factor for climate data records. For this, we use a simple method of SST retrieval, based on Planck's law and atmospheric corrections, from reprocessed homogeneous IASI radiances that can produce a consistent SST record for the period available to date (and which can be expanded easily in the future as more data becomes available). The reprocessed IASI data set and the retrieval methods are both described in the next section (Section 2). The results are presented in Section 3, where we intercompare our data set with other SST data sets and show interannual variability and trends in SST for the study period of 2008–2019. The results are discussed in Section 4, where conclusions on the suitability of our data set for climate applications is presented.

2. Data Sets and SST Retrieval Method

2.1. IASI Data and Channel Selection

In this work, we use IASI/Metop-A radiances (also called L1C data) that have been recently reprocessed by EUMETSAT (European Organization for the Exploitation of Meteorological Satellites), ensuring data homogeneity (changes in processing is one of the main sources of inhomogeneity; Karl et al., 1993). Note that skin temperature is a product available within the IASI L2 EUMETSAT portfolio, but, to date, a consistent record is not available, as the backward reprocessing with the latest version of the EUMETSAT algorithm has not been performed yet.

The IASI instrument (Clerbaux, Boynard, et al., 2009) measures radiances in the thermal infrared spectral range between 645 and 2,760 cm^{-1} corresponding to 8,461 spectral channels, every 0.25 cm^{-1}, with an instrument response function of 0.5 cm^{-1} half-width at half maximum after apodization. More than 1.2 million radiance spectra per day are provided by each IASI instrument, with a footprint on the ground of 12 km diameter pixel (at nadir) over a swath width of about 2,200 km. IASI-A (used in this work) revisits all points on the Earth's surface twice a day at around 9:30 and 21:30 local time. Metop-A satellite is now exploited on a “drifting” orbit from June 2017 onwards, in order to extend its useful lifetime from 2019 to 2022 (EUMETSAT, 2018). Local time at ascending node will be slowly decreasing from the nominal mission value of 21:30 in June 2017 to 19:30 in 2021.

To find the most informative channels to retrieve sea surface temperature from the 8,461 IASI channels, a simple method, based on the Jacobians of brightness temperature, is used. This method simulates a set of spectra representative of IASI measurements (i.e., season, location, atmospheric composition), and statistically analyses their Jacobians, which measures the sensitivity of the IASI measurements with respect to the surface temperature, at each wavenumber. Clear sky spectra are used in order to access information at the surface.

Spectra were simulated using the RTTOV (Radiative Transfer for TOVS; Saunders, Hocking, Turner, et al., 2018) code (version 12.1), using meteorological parameters from ECMWF and chemical parameters from the Copernicus Atmosphere Monitoring Service (CAMS; https://atmosphere.copernicus.eu/) (Tables S1a and S1b). The spectral emissivity over the sea is calculated directly in RTTOV, based on the IREMIS model (Saunders, Hocking, Rundle, et al., 2017) which is parameterized in terms of zenith angle, surface wind speed and skin temperature. The RTTOV code is run on 2 days: a day in boreal winter (January 1, 2017) and summer (June 1, 2017); at 9 a.m. and 9 p.m. (approximately around the crossing time of IASI), for a ±7° longitude band centered on the zero longitude, gridded to a 1° × 1° resolution. This amounts to a total of $\sim 10^4$ geophysical scenes to analyze. After selecting the simulations over the sea, we calculated the average surface temperature Jacobian spectrum obtained from these spectra. In this Jacobian spectrum, we first select two spectral bands associated to the highest signal-to-noise ratio: the (800–1,000) cm^{-1} spectral

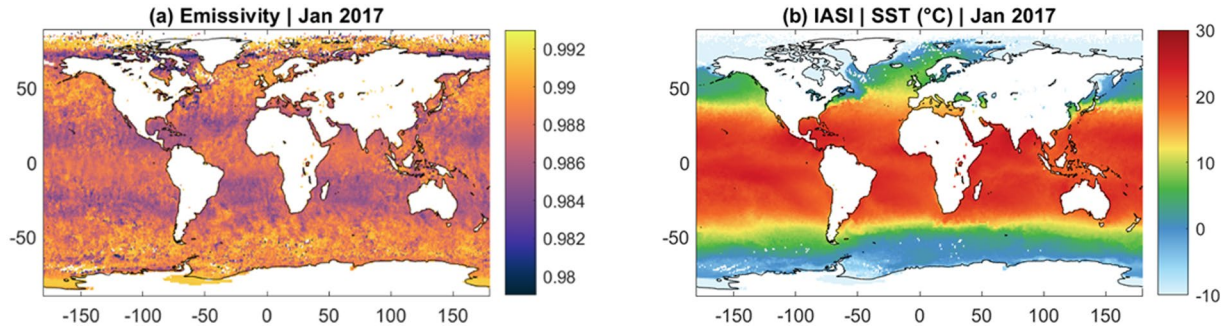

Figure 1. (a) Monthly mean emissivity for January 2017 averaged over a 1° × 1° grid; (b) corresponding monthly mean SST over the ocean retrieved from IASI radiances averaged over a 1° × 1° grid.

band and the (1,060–1,260) cm^{-1} band. Then the channels with maximum values (i.e., the values the closest to a low frequency envelope function representing the upper limit of the average Jacobian spectrum) were selected in these two bands. In order to limit the number of selected channels to about 100, the channels are first filtered to the 0.5% closest to the upper limit function in the (800–1,000) cm^{-1} spectral band, and 2% in the (1,060–1,260) cm^{-1} band. A second filtering is applied by splitting the spectral band into 10 subbands of 10–15 cm^{-1} and determines the channels with the highest spectral correlation with the channel the closest to the Jacobian upper limit function. In the end, 129 channels were selected. These selected channels are shown in Figure S1 as black crosses superposed on a typical IASI spectrum, and the actual values are presented in Table S2.

2.2. Emissivity Over the Sea

At each of the selected channels, the temperature, T, can be computed for each cloud-free scene (cloud cover under 10%, using the L1c IASI cloud flag derived from synchronized AVHRR, measurements at each IASI spatial foot print) as a function of the radiance by using the inverse of Planck's function (Equation 1):

$$T = \frac{h \cdot c \cdot x}{k \cdot \log\left(\frac{2 \cdot \epsilon \cdot h \cdot c^2 \cdot x^3}{L} + 1\right)} \tag{1}$$

where x is the wavenumber, L is the radiance, $k = 1.3806e{-}23$ $J \cdot K^{-1}$, $h = 6.6262e{-}34$ J·s, $c = 2.9979e + 10$ $cm \cdot s^{-1}$, and ϵ is the emissivity of the surface. Over the sea, in the thermal infrared spectral range, the emissivity depends on the wave number, the satellite scan angle, and the roughness of the sea surface (e.g., Masuda et al., 1988). For the wavenumbers and scan angles in this study, the emissivity varies roughly between 0.98 and 0.99. Past studies have used constant values for the emissivity over the sea (e.g., Konda et al., 1994) or have used emissivity models (e.g., Wu & Smith, 1997). In this work, we use a lookup table-based method, taken from Nalli et al. (2008). In this method, each interval in wavenumber, satellite angle, and wind speed corresponds to a value of surface emissivity. The wind speed in this case was computed from the European Center for Medium-Range Weather Forecasting (ECMWF) latest reanalysis (ERA5) u and v wind components at 10 m, matched spatially and temporally to the IASI observations. ERA5 is a state-of-the-art reanalysis from ECMWF, which uses advanced models to assimilate vast amounts of satellite and in-situ data (Hersbach et al., 2020). ERA5 has an hourly temporal resolution re-gridded to a regular grid of 0.25° × 0.25°. This is a simple, straightforward method that provides us with a way to compute surface emissivity.

For each IASI observation, we first find the corresponding u and v wind fields from ERA5 and then using the lookup table, for each channel, we find the corresponding emissivity. After, the temperature is computed at each observation, for each channel, before being averaged in time and space. An example of the monthly mean emissivity computed using this method for January 2017, averaged over a 1° × 1° grid is shown in Figure 1a. Although emissivity over the ocean exhibits a clear spatial variation, the range of values is limited

to between around 0.984 and 0.992. Figure 1b shows the monthly mean SST for January 2017, with the well-known pattern of SST with maxima over the tropics and decreasing temperature toward higher latitudes. In the temperature retrieval, the biggest source of uncertainty is the emissivity, so the derivative in relation to emissivity ($\partial T/\partial e$) was computed. For our range of channels and radiances, and considering an emissivity of 0.985 (and the constants defined above), the uncertainty is between 0.05 and 0.5 K.

In order to study large-scale trends and variability in SST across oceans, we averaged the IASI observational record on a monthly $1° \times 1°$ grid. Given that IASI day and night measurements are taken at around 9:30 a.m. and p.m., local time, we choose in this work to average both observations for easier comparison with the other data sets. According to Robinson (2004) and Merchant (2013), these trends and variability occur on time scales of months to years, and on spatial scales of 500–5,000 km, in the case of interannual variability. Therefore, they are captured by these spatial and temporal resolutions (while simultaneously keeping our analysis computationally efficient).

2.3. Water Vapor Attenuation and Correction

The SST data was first compared with ERA5 (Hersbach et al., 2020). ERA5 is a state-of-the-art reanalysis, with a stability over time that a product like the L2 from EUMETSAT could not provide (as we will show in the next section). Although ERA5 may have issues in certain regions, such as tropical East Africa (Ssenyunzi et al., 2020), it has global 1-hourly coverage, at a 0.25° resolution, which makes it appropriate and convenient to interpolate to the time and location of the satellite observation. In ERA5 the surface temperature over the ocean is computed from an analysis by the Operational Sea Surface Temperature and Ice Analysis (OSTIA, McLaren et al., 2016). Their SST analysis blends satellite and in situ observation with the resulting SST representing the foundation SST fields (i.e., measured a few meters deep; which can be assumed as the same as sub-skin at night, when SST is free from diurnal variability). Since the ocean skin temperature is measured at about 10 μm thickness, parameterizations of different near surface ocean effects (i.e., cool skin effect due to turbulent and long wave radiative heat loss to the atmosphere; warm layer effect due to low winds and solar radiation; and salinity effects on the saturation of specific humidity at the surface) are included in the code to determine the skin temperature over the ocean (ECMWF, 2016; Hirahara, et al., 2016). Using ERA5, we calculated the mean difference between skin and sub-skin SST and the results show that the skin SST is generally cooler than sub-skin SST by 0–0.2°C (not shown here).

This comparison shows an overall negative bias with IASI-derived SST (Figures 2a and 2b), which is highest over the tropics. Over the tropics the pattern of the bias is close to the structure of mean integrated water vapor (IWV, i.e., total column water vapor in mm), shown in Figures 2c and 2d. There is a high correlation between the bias and IWV, with the regions of maximum bias corresponding to the areas where the water vapor is also highest. In the thermal infrared, the water vapor continuum contaminates the whole spectral domain. Although we attempted to choose the best channels for SST retrieval, the prevalence of emitting/absorbing water vapor at all channels is responsible for a signal attenuation that produces an overall negative bias in the SST estimates that needs to be corrected.

Corrections of the water vapor attenuation have been extensively discussed in previous studies, and several atmospheric correctors have been used. From split window retrieval methods (McClain et al., 1985; Walton et al., 1998), and adaptations using additional channels in the near infrared, to nonlinear estimators (Barton, 2011; Emery, Yu, et al., 1994; Kilpatrick et al., 2001; Li et al., 2001; Minnett, 1990) to approaches involving radiative transfer modeling (Merchant & Le Borgne, 2004) and optimal estimation (Merchant, Le Borgne, et al., 2008).

In this work, the goal was to use an easy and quick method that could be applied to the monthly mean data. In order to remove the IWV contribution, we started by computing the SST bias as a function of IWV from ERA5 and performing a quadratic fit on the data for each month and year (as this relationship varies throughout the year and to a lesser extent from year to year). An example of the bias fit is given in Figures 3a and 3b for January 2017 and July 2017. In this study, results for January and July will be shown, in order to illustrate the maximum seasonal range. This bias due to IWV is then removed from our previous estimation of SST and the resulting SST fields are shown in Figures 3c and 3d. They show an increase in the temperature in comparison with the previous estimate, especially in the tropics. When we compared the corrected

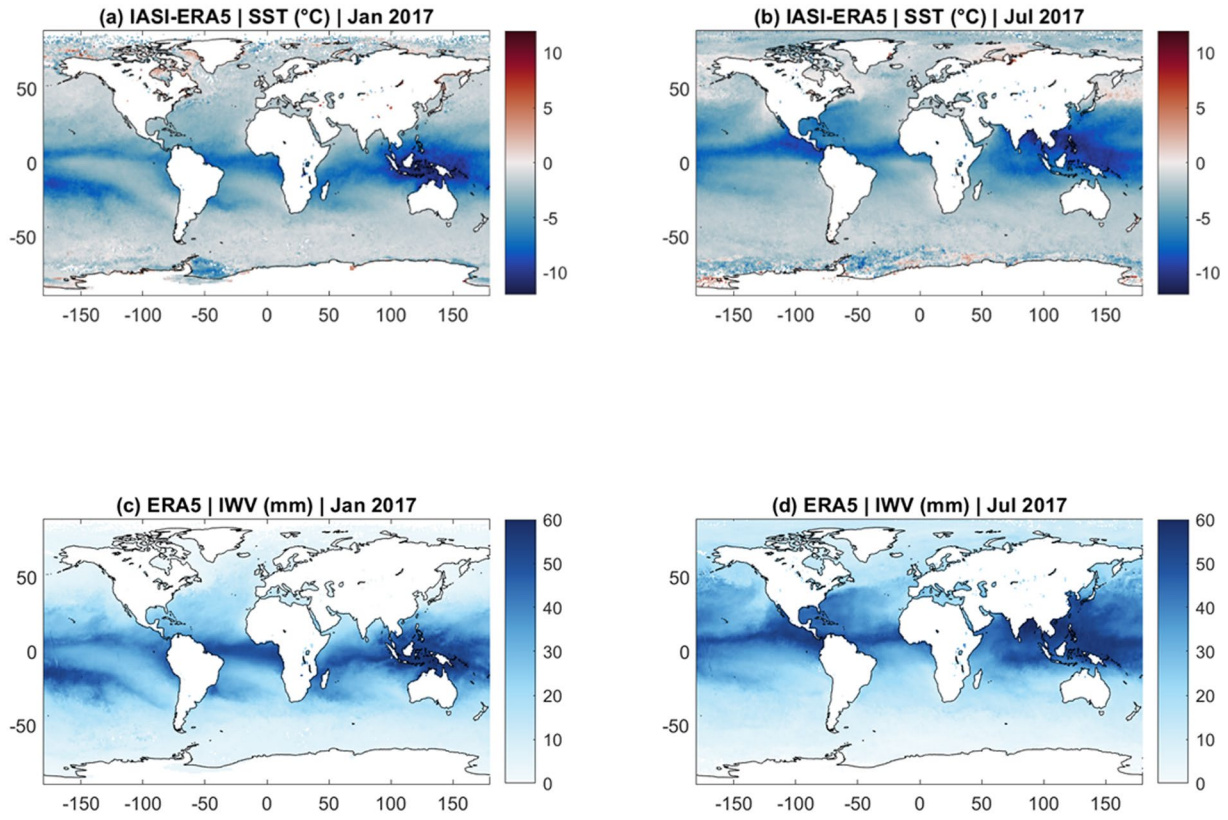

Figure 2. (a) Difference between IASI-derived SST and ERA5 SST for January 2017; (b) Same as (a) but for July 2017; (c) Monthly mean IWV for January 2017; (d) Same as (c) but for July 2017.

SST with the first guess SST, similar differences as the difference between first guess SST and ERA5 were found (not shown). The uncertainty in the corrected SST depends on the IWV, so ∂SST/∂IWV was computed. For a range of IWV values from 0 to 60 kg/m^2, the uncertainty is between around 0.05 and 0.45 K.

The signal attenuation of the infrared radiation emitted by the sea surface due to water vapor is known to be the largest error source in the conversion of SST from infrared satellite data. Other error sources are the presence of clouds (which we attempt to minimize by choosing only cloud-free scenes), other radiatively active gases (e.g., carbon dioxide, nitrous oxide, methane; which we limit by carefully selecting the best channels) and aerosols (absorbing, emitting radiance, and may also scatter it). The concentration of aerosols is more variable and their radiative properties less well understood than for water vapor and other gases. The impact of aerosols on SST computations can range from insignificant (in clean air conditions) to highly significant (in, for instance, dust storms). Although the impact of aerosols will not be corrected in our data set, it will be considered when interpreting the results, especially in regions prone to the effect of dust storms, such as the Persian Gulf and off the coast of West Africa.

Once this method of retrieving SST from IASI radiance data was established, it was applied to the entire period of available reprocessed IASI data (2008–2019). In addition, at higher latitudes, our data set covers areas that contain sea ice (e.g., areas where SST is negative in Figures 3c and 3d). Since our method does not account for this (the emissivity of the ice is different from the emissivity of the ocean), we removed these areas from our data set, using ERA5 monthly mean sea ice concentration fields. The resulting data set was compared first with ERA5 and IASI L2 (provided by EUMETSAT) skin temperature over the ocean (skin SST, but henceforth referred to as SST for simplicity) data for validation, and second with two independent and well-documented SST climatological data sets to assess its suitability for climate studies.

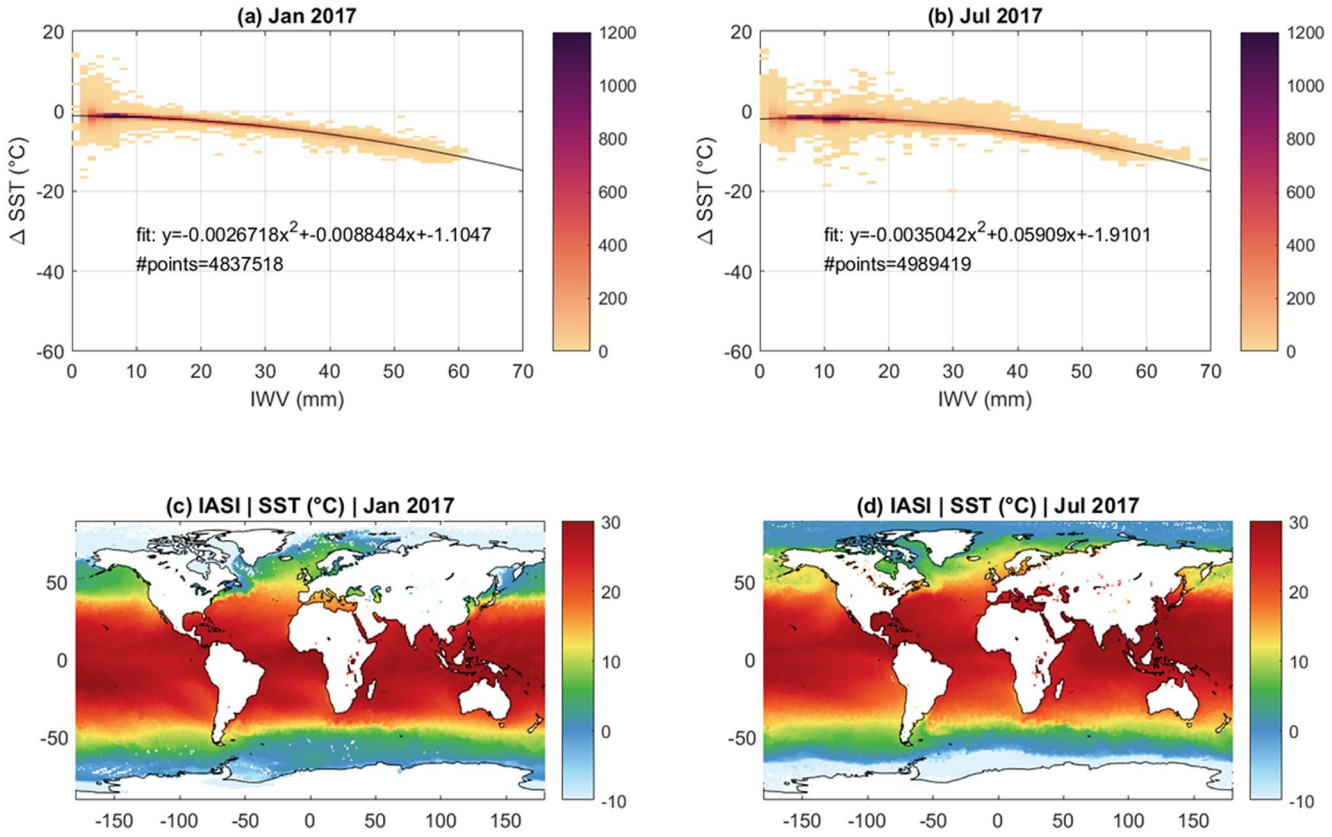

Figure 3. (a) SST bias fit as a function of IWV for January 2017; (b) Same as (a) but for July 2017; (c) Corrected IASI-derived monthly mean SST for January 2017; (d) Same as (c) but for July 2017.

3. Results

3.1. Assessment of IASI-Derived SST Data Set

For the validation of our IASI-derived skin SST data set (henceforth referred to as IASI SST), we compared mean discrepancies and SD of discrepancies between our data set and the skin temperature over the sea product from ERA5 (as described in the previous section, and referred to henceforth as ERA5 SST) and IASI L2 skin SST from EUMETSAT (referred to as L2 SST). Note that our SST data set was not directly compared with reference in situ data such as drifting buoys, as this is sub-skin SST data. On the other hand, reanalysis skin temperature data is available at relatively high spatial and temporal resolution. For climate applications, an important quality to consider is stability (i.e., constancy) in these discrepancies statistics (e.g., GCOS, 2006), more so than accuracy at a particular instant, and the variability structures at a global scale.

The EUMETSAT L2 SST product (IASI Level 2 PPF [Product Processing Facility]) is the skin temperature product over the sea derived primarily from IASI for cloud-free scenes. For cloudy scenes, it uses the advanced microwave sounding unit (AMSU), and the microwave humidity sounder (MHS), which are synchronized with IASI's scanning (EUMETSAT, 2017a, 2017b). This SST product is also available for all cloud cover unlike our data set, and is therefore more complete. However, the processing used to derive the skin temperature has evolved over time, and as a result this data set has discontinuities (Bouillon et al., 2020), which will be shown in this section.

Figures 4 and 5 show the mean temperature differences between IASI SST, L2 SST, and ERA5 SST for 2008 and 2017, for January (Figure 4) and July (Figure 5). In January, the differences between the IASI SST and ERA5 SST are generally under 1°C, with a positive difference over the Equator and south of 50°S and a generally negative difference elsewhere. There seems to be a much larger bias in the tropics in 2017 compared to 2008, and an inversion of the bias around the gulf stream. These can be due to a couple of reasons: on the

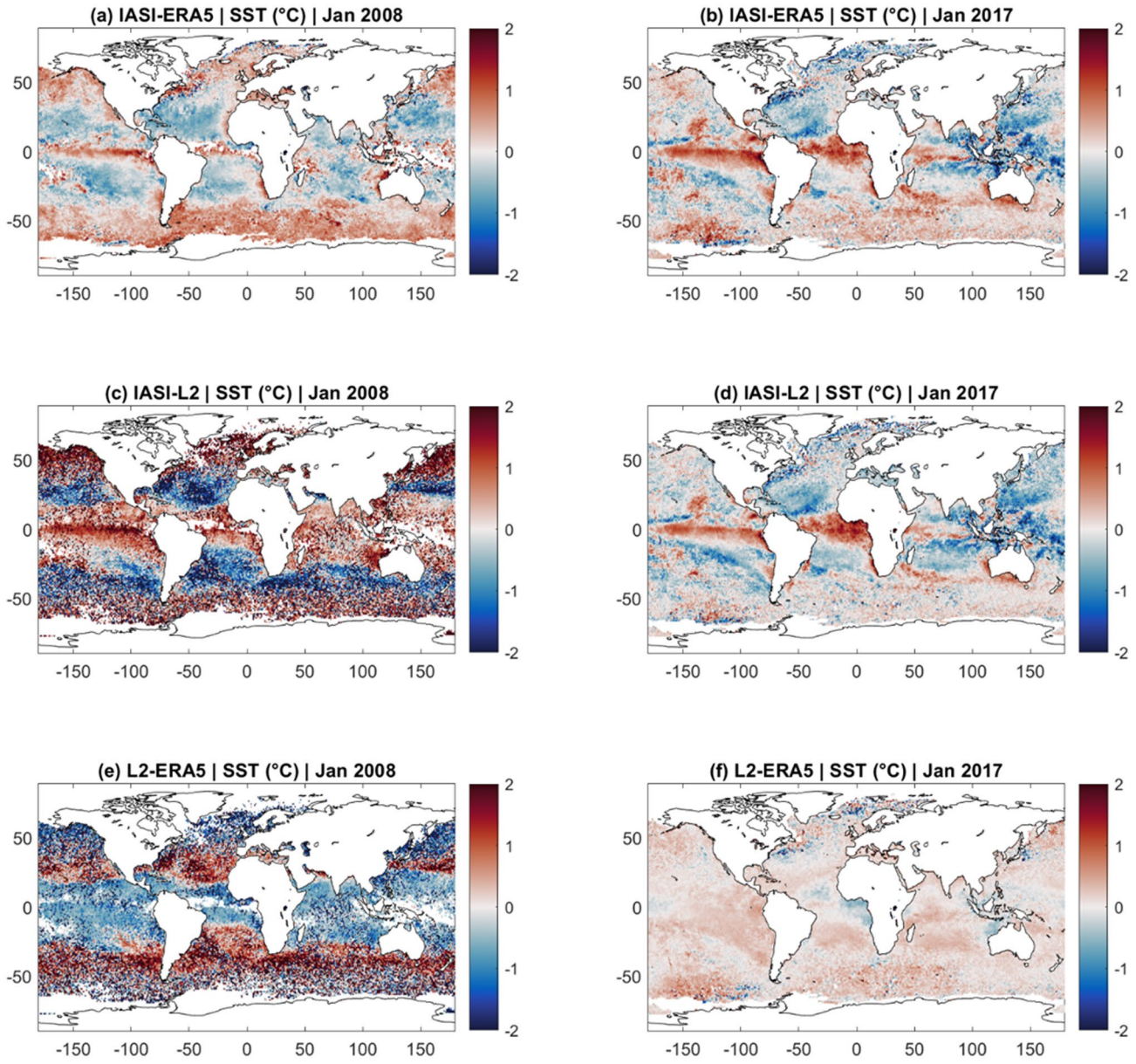

Figure 4. Mean SST differences between IASI and ERA5 (a), (b), IASI and EUMETSAT L2 data (c), (d), and EUMETSAT L2 and ERA5 (e), (f) for January 2008 and 2017.

one hand, the lack of points in some regions along the Equator in 2008 due to the cloud cover we are using (2008 has less clear sky measurements, with gridpoints with no measurements); on the other hand, it may be due to the IWV correction. These points may fall further from the curve fit between IWV and SST, and may therefore be over/undercorrected in some years. In July, positive differences are higher around 50°N. The pattern and order of magnitude of the biases are approximately the same for 2008 and 2017.

The differences between IASI SST and L2 SST products are of the same order of magnitude as the differences between IASI SST and ERA5 SST (and show a similar spatial pattern) for both months in 2017 when the L2 SST retrieval is most up to date. However, for 2008, the differences reach higher values (up to 5°): there is a general warm bias in IASI SST for July 2008, and a warm bias over the tropical and higher latitudes in January 2008. There is a clear decrease in the differences between IASI SST and L2 SST data from 2008 to 2017, which is consistent with the clear decrease in the bias between L2 SST and ERA5 SST from 2008 to 2017.

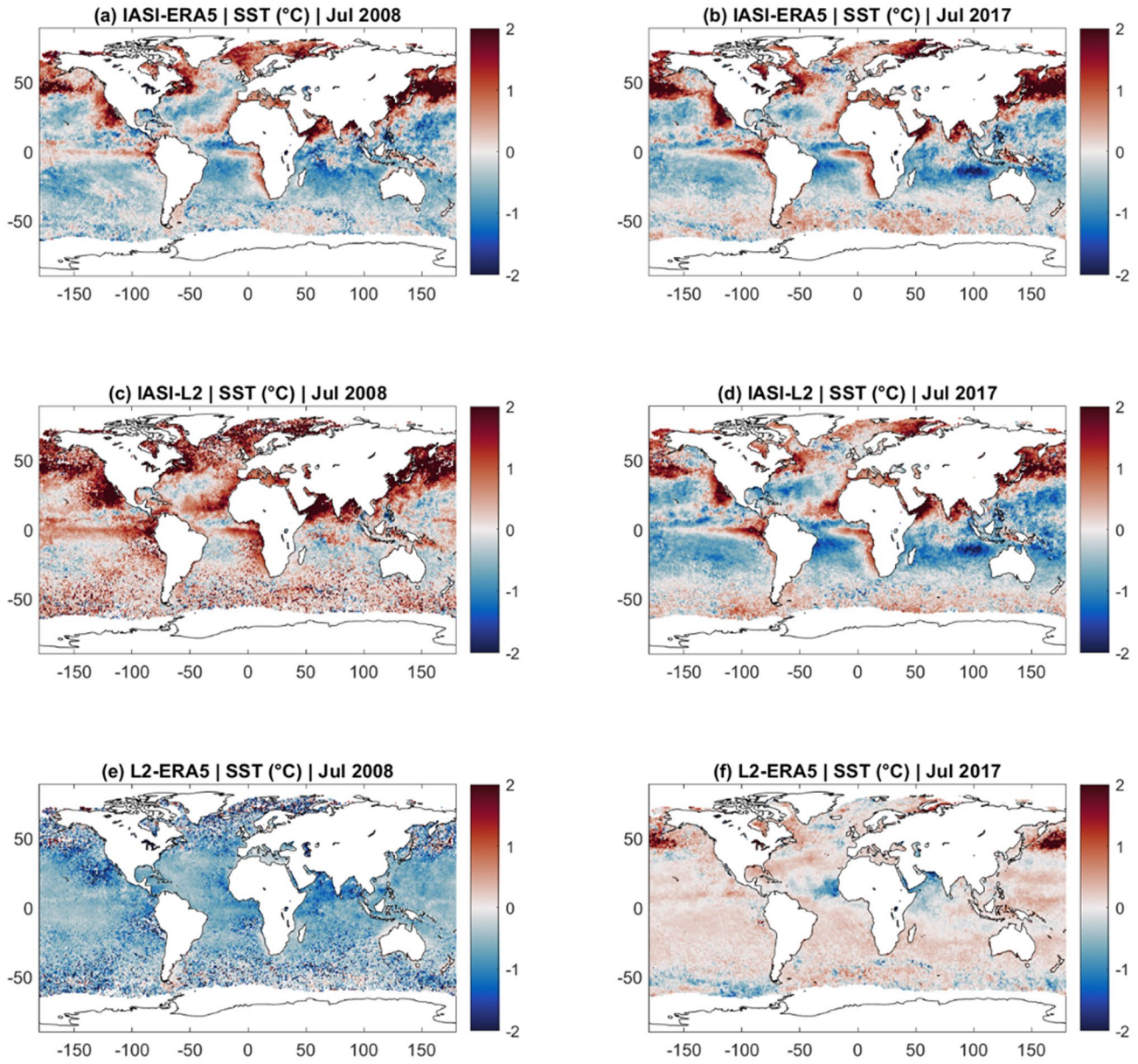

Figure 5. Same as Figure 4 but for July.

Figures 4 and 5 show that the L2 SST data is inconsistent in time, which is explored hereafter. This discontinuity in the L2 SST data would impede its use in climate studies, and hence the advantage of the IASI SST data set computed in this work. In fact, several changes in the L2 SST data processing have been reported, which have impacted the SST estimates. These changes include changes in the clouds (e.g., cloud detection algorithms), spatial resolution (i.e., inclusion of both even and odd IASI pixels starting in March 2010), retrieval and processing algorithms (Van Damme et al., 2017).

We extend our analysis over the entire 2008–2019 period and plot the impact of the L2 SST product updates, with respect to the reference ERA5 SST data set. Figure 6 shows the evolution over time of the globally averaged SST bias and SD for the IASI SST and L2 SST, with respect to ERA5 SST.

According to Figure 6, while the bias and SD remain approximately constant in the IASI/ERA5 comparison, it clearly varies interannually in the L2/ERA5 comparison. With time, and in particular after 2015, the L2

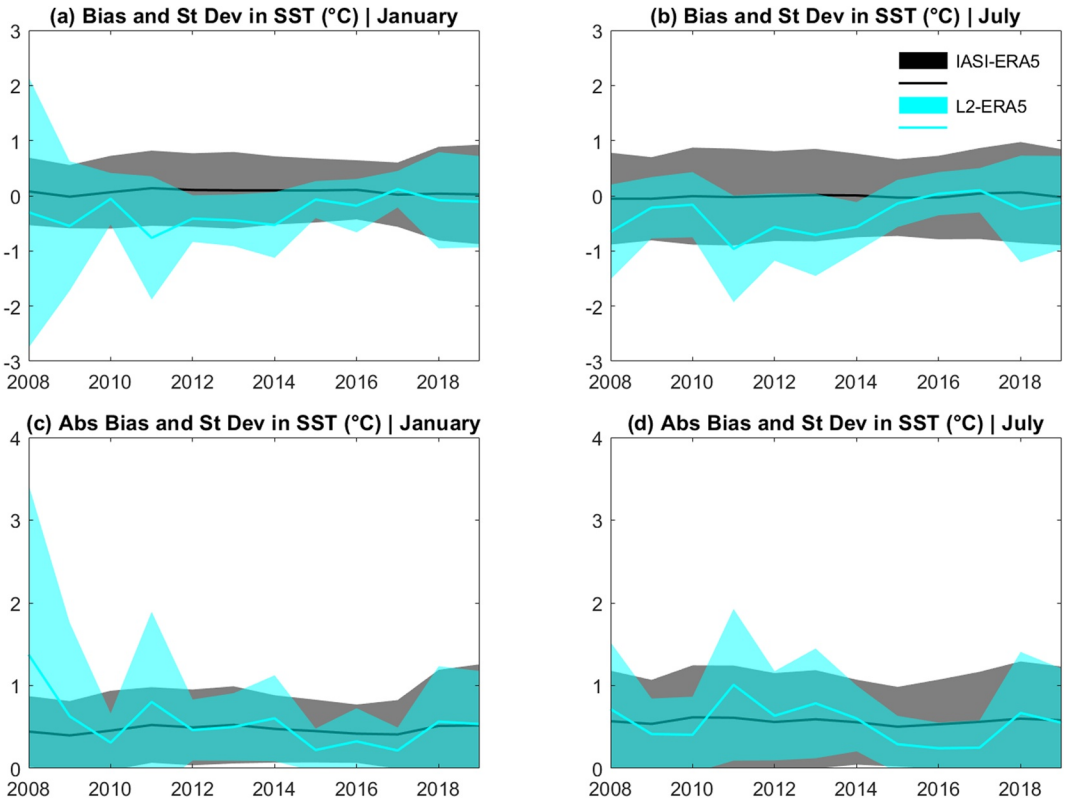

Figure 6. (a) Evolution of the bias (IASI-ERA5 and EUMETSAT L2-ERA5) and its SD (in shaded color) in SST over time for January; and (b) for July; (c) Absolute bias of differences with SD (in shaded color) for January; and (d) for July.

SST product values approach those of ERA5 and there is a clear decrease in the bias and SD, consistent with changes in the data processing.

The bias in the IASI SST data set is ~0°C for both January and July, with absolute biases close to 0.5°C throughout the entire period (check Table S3 for the actual values). For the L2 SST data there is an overall decreasing trend in both bias and absolute bias, with increases and decreases through the years. For instance, there is a steep decrease in the absolute bias from 1.5°C in January 2008 to 0.8°C in January 2009 that might have been due to major changes in cloud coverage, surface temperature, and temperature profiles reported for April 2008 (Van Damme et al., 2017). The bias continued to decrease from 2009 to 2010 as surface temperature is only provided for the cloud-free observations. From 2010 to 2011 there is an increase in the bias. During 2010, the number of cloud-free observations was increased and later temperature information started being provided for cloudy pixels. From 2011 to 2012, the bias decreases again with the improvement of cloud screening for temperature retrievals in October 2011. In September 2014, there is a major update in the processing algorithm with the arrival of a new IASI L2 processor, which is followed by a slight decrease in the bias. In January 2016, there is a peak in the bias following updates to the surface temperature algorithm in September 2015. By July 2016, the bias has decreased due to important improvements in the temperature retrieval algorithms from May 2016 onwards.

The SD of the differences between the IASI SST and ERA5 SST remains approximately constant throughout the period at study, at around 0.6–0.8°C in both January and July, while the differences in SD of both data sets is ~0.2°C. This shows the variability in both data sets is approximately the same. For the L2 SST data set, the SD of the difference with ERA5 shows an overall decrease over time. For January, the SD of the difference goes from about 2°C in 2008 to less than 0.5°C in 2017. For July, it drops from about 1°C in 2008 to less than 0.5°C in 2017. There are also increases at some years: January 2011, 2014, and 2016, and July 2011 and 2013 that are consistent with some of the changes in the L2 SST data highlighted before. The difference

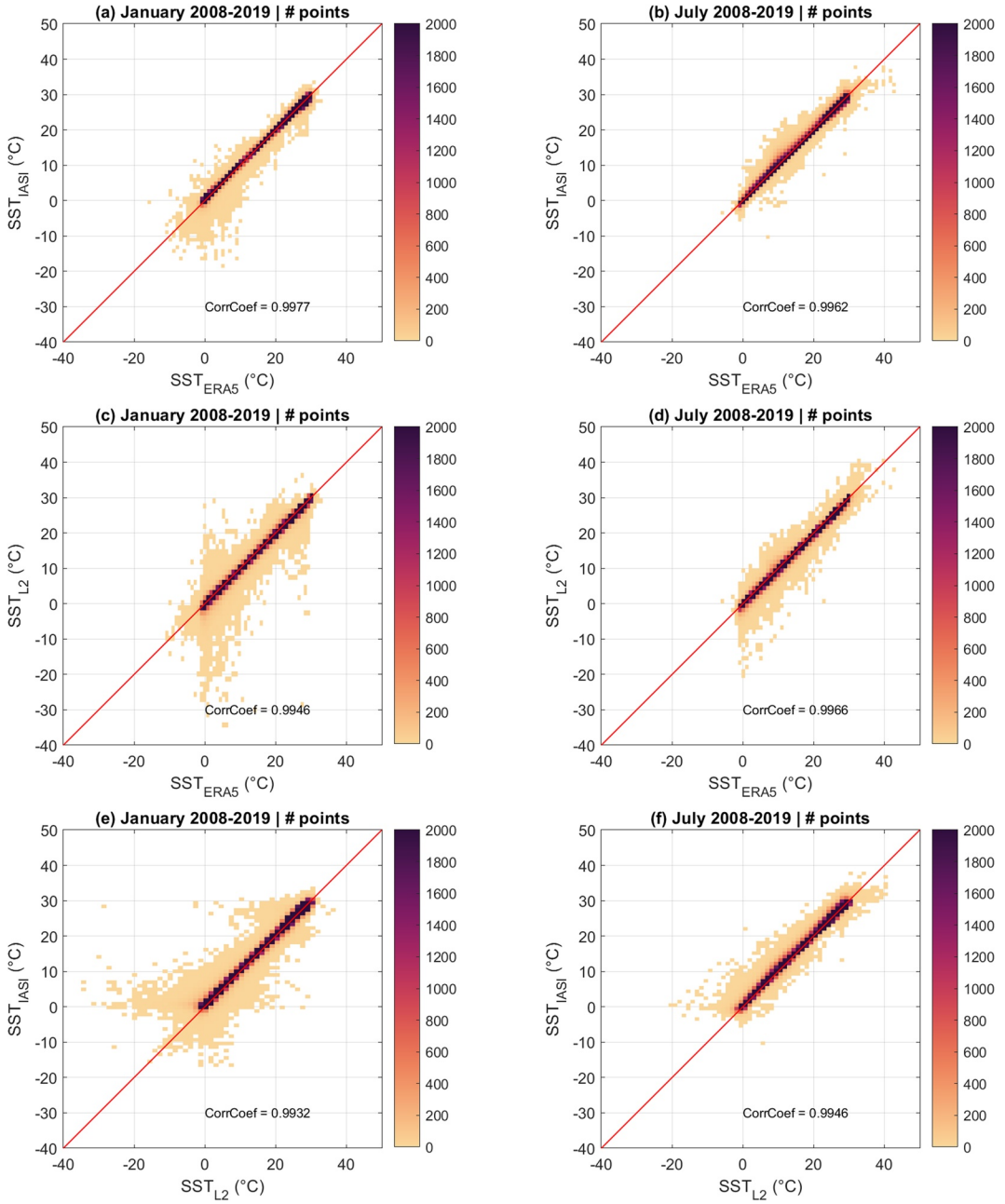

Figure 7. Scatterplots of the correlation between pairings of the three data sets: IASI, EUMETSAT L2, and ERA5. The correlation is chosen at all months of January and July of 2008–2019 (12 months), separately to highlight the seasonal variation.

in SD between L2 SST and ERA5 SST is negative throughout the entire period, and decreases over time. This means the variability in SST was underestimated in the L2 data, especially until July 2014 (and January 2015). Although it is not shown, there are also differences between the bias and SD time series at different latitude bands. The absolute bias is higher for the 30–60°N latitude band, especially in July, and the SDs are also higher for this latitude band.

Figure 7 shows the correlation between pairings of the three data sets. The correlation is chosen at all months of January and July of 2008–2019 (12 months) separately to highlight seasonal variation. Although the correlation between all three SST data sets is high, with correlation coefficients close to 1 (over 0.99),

there is a bigger dispersion in the L2 SST over the entire period in Figure 7, especially for January. This corresponds to the higher differences (in IASI and ERA5 vs. L2) discussed above for the beginning of the period, and further highlights the need for a consistent data record.

Table S3 shows a summary of the results presented above, averaged over the entire period. It reiterates that our IASI-derived data set has a low bias and SD and high correlation, when compared with ERA5 SST and L2 STT. Since the IASI SST bias due to water vapor is corrected using the IWV in ERA5, the global mean bias is close to zero. Although our data set depends on ERA5 for wind fields and water vapor correction (constant over 1 month), it is essentially driven by IASI radiances. The retrieval, even if obtained using reanalysis, does not reproduce the reanalysis, as the temporal and spatial variations are still driven by the satellite observations.

3.2. Comparison with Other Independent SST Data Sets

To assess the quality of our data set for the study of variability and trends we also compare our data set with independent SST measurements. These are: NOAA's Optimal Interpolation SST (Reynolds et al., 2002) and Hadley Centre's Global SST (Rayner, Parker, et al., 2003), that have been extensively used in climate studies. Our SST data set is cloud-free. In order to check the impact of the data gaps (in space and time) on our data, the IASI SST monthly mean fields were also compared in this section with the full (i.e., not matched) ERA5 SST data set in terms of SD and trends.

The Hadley Centre Global Sea Ice and Sea Surface Temperature (HadISST version 1.1) is a combination of monthly globally complete fields ($1° \times 1°$) of SST and sea ice concentration that is available from 1871 to the present. The HadISST uses reduced space optimal interpolation applied to SSTs from the Marine Data Bank (mainly ship tracks) and adjusted satellite-derived SST data from 1982 onwards (monthly SST from NOAA's operational AVHRR instruments). SST for grid cells partially covered by sea ice is estimated from statistical relationships between SST and sea ice concentrations (Rayner, Parker, et al., 2003).

The NOAA Optimal Interpolation SST analysis, version 2 (OISSTv2) is a global gridded ($1° \times 1°$) data set, computed from a combination of ocean temperature observations from satellite (AVHRR) and in situ platforms, such as ships and buoys (moored and drifting). Because the input data are irregularly distributed in space, they are first placed on a regular grid, before statistical methods (i.e., optimum interpolation) are applied to fill in missing values. The methodology used to create this data set includes a bias adjustment step of the satellite data to in situ data prior to interpolation (Reynolds et al., 2002).

These data sets are combinations of different observations and observation types (e.g., satellite and in situ) that vary over time, as different data sets become available. Our data is based on information from one instrument only, and therefore will not suffer such changes and will produce homogeneous data more easily. This makes it a good data set for other more complex data sets to be compared against, provided that it can estimate the trends and variability correctly. However, it needs to be taken into account that while our SST data set is skin SST, HadISST, and OISSTv2 are sub-skin SST data sets.

3.2.1. SST Interannual Variability

Figure 8 shows the SD in January SST from 2008 to 2019, for IASI, ERA5, OISSTv2, and HadISST and Figure 9 shows the same, but for July. Note that we use the full (not IASI-matched) ERA5 SST data set in order to assess the impact of cloud cover, and spatiotemporal interpolation on our data and to keep a similar comparison method for the other two data sets.

For both months, it is clear that in general, the IASI SST data set has a higher variability globally, while the HadISST has generally a lower variability. The larger noise in some areas for the IASI SST data set (especially in July in the northern hemisphere) could be due a sampling issue. Because in the IASI data set only clear pixels are selected, the gaps in the data due to cloud cover might create an artificial higher variability. The regions where the variability in IASI is higher than for the other data sets (especially in the Northern Hemisphere, in the Northern Pacific ocean) do coincide with the regions where total cloud cover is close to 1/100% (not shown).

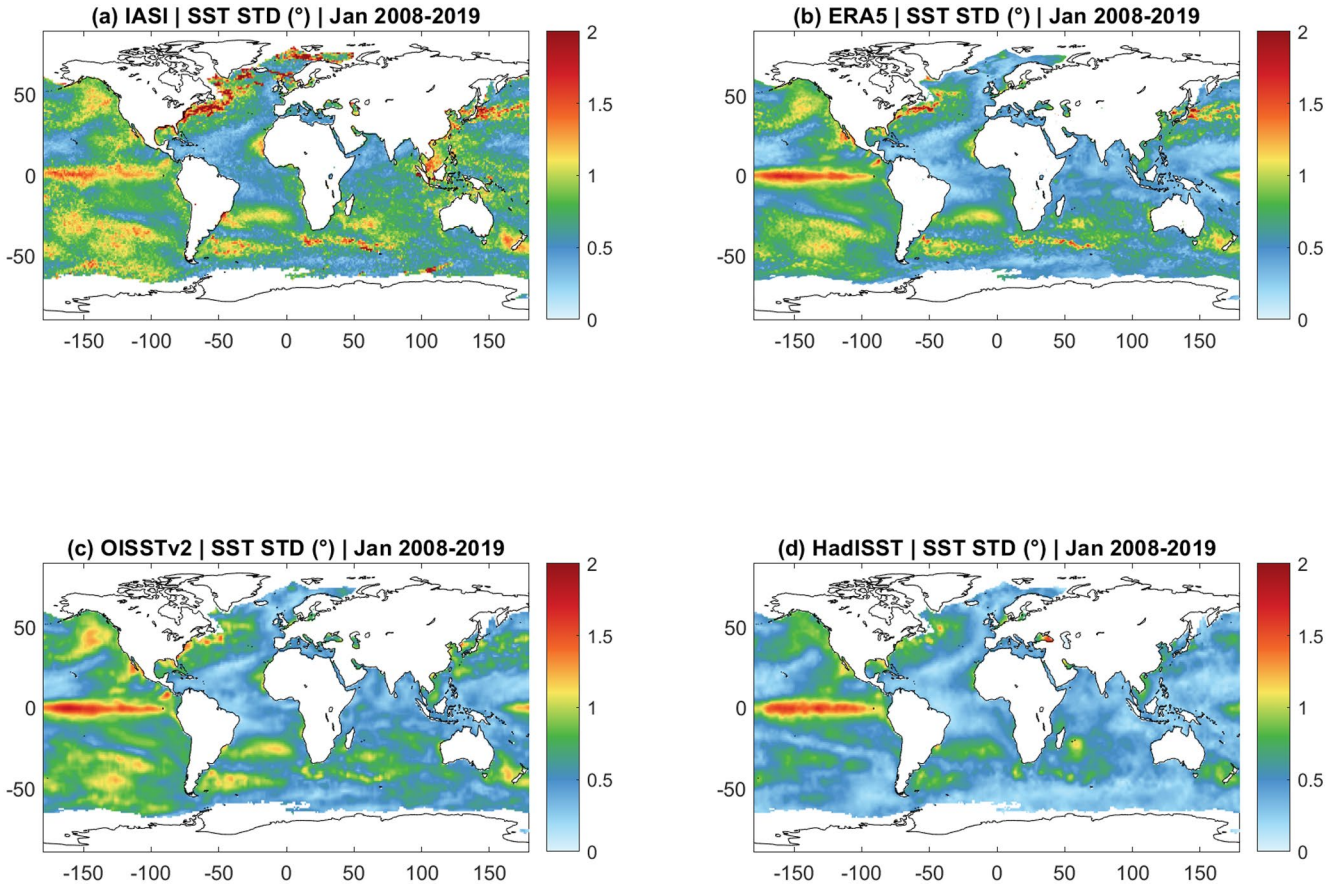

Figure 8. Monthly mean SD in SST for January 2008–2019, for IASI, ERA5, OISSTv2, and HadISST.

For January, there is a clear high variability translated with a SD that exceeds 1.5°C in the tropical Pacific region in all data sets, due to the ENSO, which is most intense during the months from December to February. The ENSO is the strongest internal climate mode at the interannual timescale, and consists of SST excursions in the central and eastern equatorial Pacific (Latif & Keenlyside, 2009). We investigate SST/ENSO relationship further in Figure 10.

There are also other regions of high variability that are present in all four data sets (although less intense for the HadISST). For instance, in the northern Pacific the SD in SST exceeds 1°C in IASI and ERA5 and OISSTv2. This is due to the interannual changes in the surface transport and path of the Kuroshio Extension System (Qiu, 2000). According to Qiu (2000), SST in this region is colder (warmer) when the surface transport is weaker (stronger) and southerly (northerly). Ocean dynamics also play a central role in the interannual variability of SST over the Gulf Stream extension (Wills et al., 2016) in the northern Atlantic, which is most intense in the IASI and ERA5 data sets. Other regions where the SST interannual variability exceeds 1°C are the South Pacific, off the coast of West Africa, in the southern Atlantic and off the east coast of South America, and in the Southern Ocean from the tip of South Africa eastward into the Indian Ocean (in IASI and ERA5). The latter is also observed in July.

For July, there are also regions of higher variability common to all four data sets such as the intense variability observed in the northern Pacific and northern Atlantic (particularly high in the IASI data). SD is also high (over 1.5°C) in all data set. along the equatorial Pacific and coastal Peru, which is related to equatorial and coastal upwelling, respectively. According to Deser et al. (2010), in the tropics nonseasonal variability is higher where there is a local minimum in the long-term mean SST due to coastal and equatorial upwelling (when colder water rises from the deeper ocean to the surface).

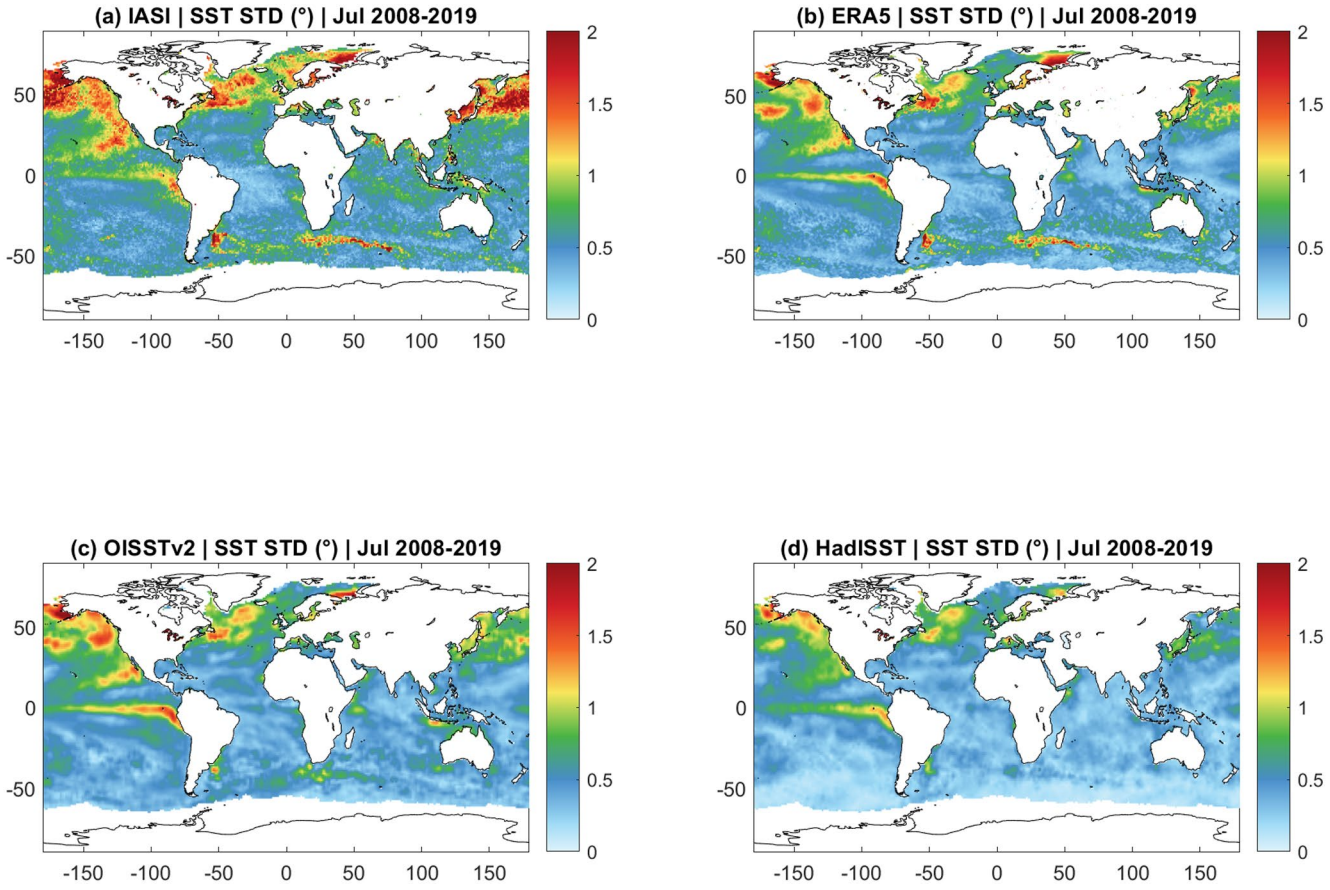

Figure 9. Same as Figure 10, but for July.

To highlight the effect of ENSO on SST, we show in Figure 10 the difference in the January SST anomalies between years of strong El Niño and La Niña. During La Niña events, there is a negative anomaly in the SST in the tropical Pacific, while there is a strong positive anomaly during the El Niño. This difference is well captured by our IASI data set (top), which shows very similar SST anomaly structures to ERA5 albeit slightly noisier, probably due to lower number of points in our clear-sky data set.

3.2.2. SST Trends

In order to assess the trends over the past decade and for the series of data sets used in this work, we show in Figure 11 the trends in SST for the period between 2008 and 2019. The stippling over the trend fields denotes the statistically significant trends. The trends were computed using the Theil Sen method (Sen, 1968; Theil, 1992), a nonparametric statistic that computes the median slope of all pairwise combinations of points. The statistical significance of the trends was assessed using the Mann–Kendall test (Kendall, 1948; Mann, 1945), at a 10% significance level.

In general, there is good consistency between the four data sets, which show similar warming and cooling trend patterns. In all data sets, we observe a cooling trend in the subpolar Atlantic Ocean and a warming trend in the Gulf Stream region. These trend patterns are consistent with the results found by other studies and presented in the Intergovernmental Panel on Climate Change (IPCC, 2013) reports and is part of a long-term trend that has been linked with a weakening of the Atlantic meridional overturning circulation (AMOC) (e.g., Caesar et al., 2018; Dima & Lohmann, 2010). The AMOC is a system of ocean currents in the North Atlantic, and it is suspected that its weakening is linked with a freshwater anomaly in the northern Atlantic. This anomaly has been linked to irregular sea-ice export from the Arctic Ocean (Belkin et al., 1998; Dickson et al., 1988), increasing river discharge into the Arctic Ocean (Peterson et al., 2002) and meltwater and iceberg discharge from the Greenland Ice Sheet (Rahmstorf et al., 2015).

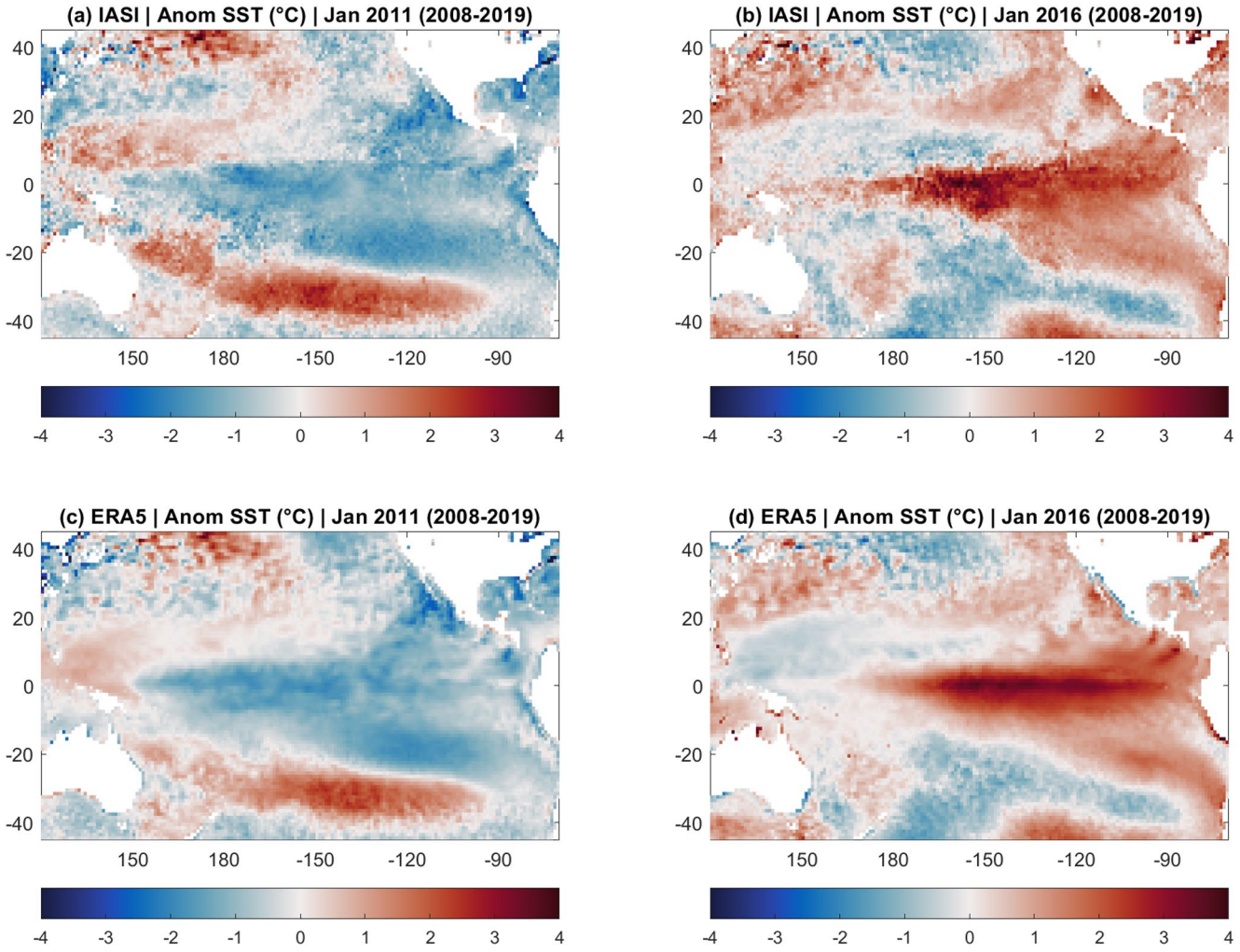

Figure 10. (a) Anomalies in IASI SST data for January 2011, in relation to the January climatology for 2008–2019; (b) Same as (a) but for 2016 SST anomaly; (c) and (d) Same as (a) and (b) but for ERA5 SST.

For all data sets, there is also a significant warming trend over the tropical Pacific and off the west coast of North America. This positive trend is part of a tripole structure in the SST trends over the eastern portion of the Pacific Ocean, which also includes a positive trend at around 50°S and a negative trend in between. This structure is present in all data sets, and is related to the ENSO. The strong 2016 El Niño event, toward the end of our study period, caused a strong warming that increased the SST trend for the tropical Pacific region. This can be seen in Figure S2, which shows the evolution of the multivariate ENSO index over the period at study (top), with the corresponding SST averaged over the latitude/longitude intervals where ENSO has the most influence. It is clear from this figure that positive (negative) ENSO indexes correspond to a warmer (colder) SST. Furthermore, the occurrence of a strong La Niña event (negative index) at the beginning of the time period, and a strong El Niño event (positive index) at the end prompted an intense positive SST trend in the region for this period.

This is consistent with Latif and Keenlyside (2009), which found that long-term trends in the Equatorial Pacific SST during the 1950–2006 period show a warming trend with a pattern that is "El Niño-like." However, other studies also suggest that trend patterns over this region are sensitive to the period at study (e.g., Cane et al. (1997) found a La Niña pattern for the 1900–1991 period) and the historical data set used (Vecchi et al., 2008). More broadly, long-term trends over the Pacific, Indian, and Atlantic Oceans have all been found to be influenced by ENSO (Compo & Sardeshmukh, 2010). Compo and Sardeshmukh (2010) have also shown it is possible to separate the trends in terms of ENSO-related and -unrelated trends, but this

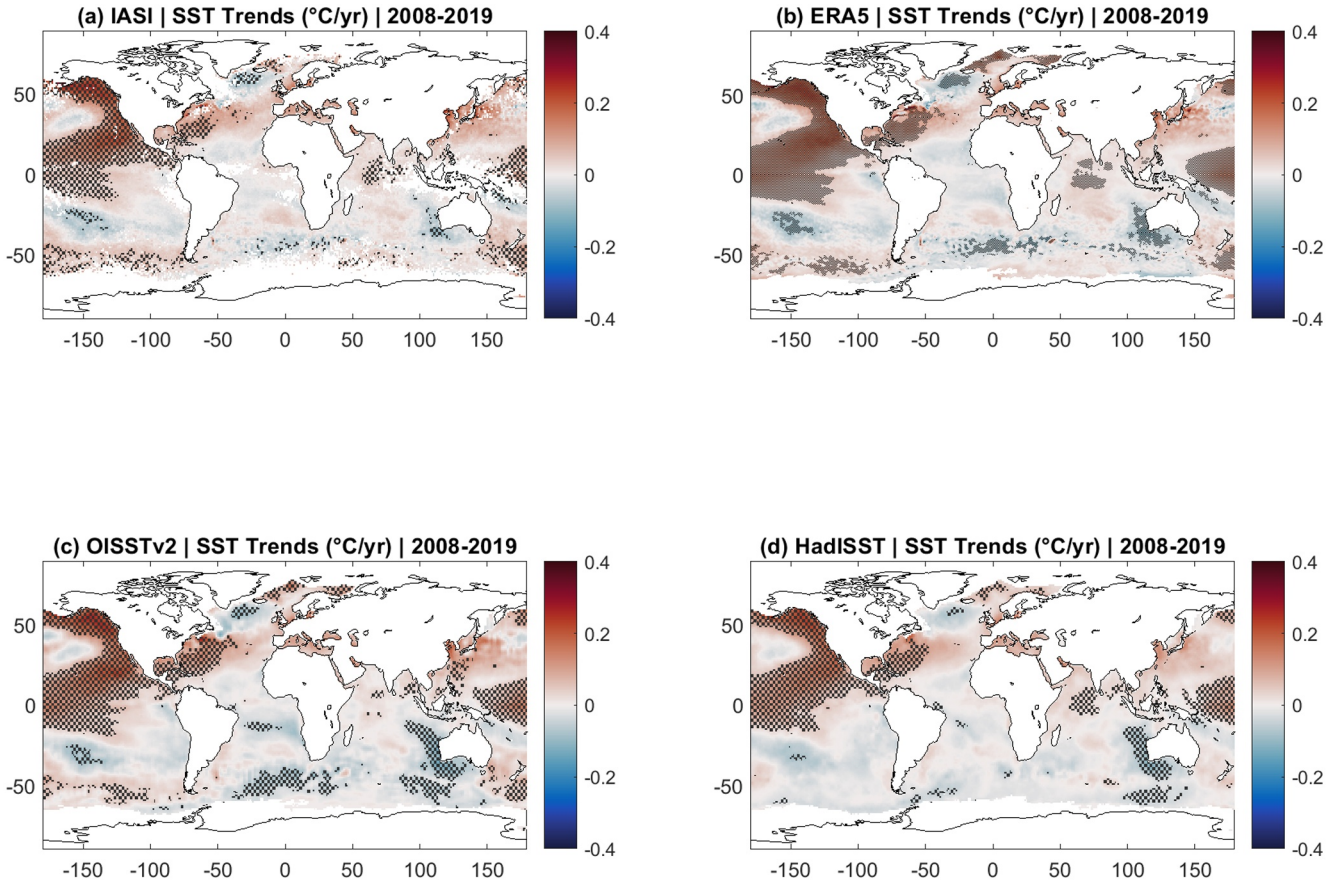

Figure 11. (a) Linear trends in IASI SST for 2008 to 2019. The stippling over the trend fields denotes the statistically significant trends at 10% significant level. (b) Same as (a) but for ERA5 SST; (c) Same as (a) but for OISSTv2; (d) Same as (a) but for HadISST.

is outside the scope of this study. Here, the goal is mainly to show that the IASI-derived data set is able to reproduce these trends accurately (i.e., show the same trend patterns as the other data sets).

There is also a note-worthy warming trend over the Mediterranean Sea that is consistent with the warming trends found for this region during the past decades in satellite and field data, as well as in model simulations (e.g., Macias et al., 2013; Nykjaer, 2009; Pisano et al., 2020; Vargas-Yanez et al., 2008). Marullo et al. (2011) first noted the influence of Atlantic Multidecadal Oscillation (AMO) over the Mediterranean Sea, then Macias et al. (2013) also evaluated the contribution of the anthropogenic induced warming during the last phase of AMO. Other significant trends found for this period include a negative trend at around 50°S in all four data sets that are not as intense/significant in the HadISST data set. Over the Southern Ocean, this data set is known to have issues resulting from sparse data input, due to the scarcity of in situ measurements in the region (Rayner, Parker, et al., 2003).

In general, there is good agreement between our data set and the other SST data sets in terms of interannual variability and trends for the 2008–2019 period. Although the period at study is relatively short, making it difficult to take physical interpretations and to compare with previous studies that have covered longer term trends, we can conclude that, in general, our data set is able to show many of the same variability and trend structures as the other more complex data sets, and capture important natural phenomena such as the ENSO well. Since our data set is based on a single instrument and consistent processing, it can be useful as a consistent record of temperature measurement.

4. Conclusions and Perspectives

In this work, we presented a reliable way of retrieving skin temperatures over the sea based on a single instrument, IASI. Temperatures were derived from the IASI satellite radiances data, based on Planck's law and simple atmospheric corrections. This method was applied to recently reprocessed IASI L1C data, in order to produce a homogeneous SST data record. This data set was first validated using ERA5 and the EUMETSAT IASI L2 data and we provide basic discrepancy statistics (mean differences, SD, and correlation coefficients). High correlation coefficients were found between the three data sets. The bias and SD in our IASI data were found to be stable over the 2008–2019 period, whereas for the IASI L2 SST, there has been a noticeable improvement over time when compared to ERA5. Overall, for the entire period, our IASI SST discrepancies with respect to ERA5 SST show a mean global bias close to zero, a mean absolute bias around 0.5°C, with a SD of difference of around 0.7°C and a correlation coefficient of over 0.99. Stability in the IASI SST is demonstrated, which is essential for climate-related studies.

Next, interannual variability and trends were compared for four SST data sets: IASI and ERA5, in addition to HadISTT and OISSTv2. It was found that our data set is able to capture the patterns of variability and trends well. Despite being noisier, the IASI SST is able to capture the same areas of high interannual variability (i.e., over 1.5°C), including over the tropical Pacific in January corresponding to the ENSO. Although the period covered by our study is not long enough to draw physical conclusions on the SST trends, similar trend patterns were found in the four data sets. In fact, although the most intense significant trends were found in the tropical Pacific due to the strong 2015/2016 El Niño, some significant trends that are part of well-documented longer-term trends were also captured by our data set. For instance, the cooling trends in the North Atlantic that are related to a slow-down in the thermohaline circulation; and the warming over the Mediterranean that is a combination of natural oscillation (AMO) and anthropogenic climate change.

In general, we have shown that the IASI SST data set described in this study is suitable for climate studies, as it produces results comparable to more sophisticated SST data sets, although some limitations need to be kept in mind. On the one hand, our data set is a skin SST data set, which is different from the sub-skin SST by up to around 0.3°C, depending on the region (the skin effect is estimated to be 0.17°C at nighttime for wind-speeds over 6 m/s, according to Donlon, Minnett, et al. [2002] and Horrocks et al. [2003]). On the other hand, it is a clear-sky data set that only includes data under (near) cloud-free conditions. Improvements to the algorithm are possible, such as looking into removing the impact of the viewing angle and the lower troposphere temperature gradients. In addition, the method described here does not correct for aerosol contamination, and does not include areas with sea ice. Still, as it is based on a single instrument, our data set can remain stable over time, ensuring that as more data becomes available, it can be used to, for instance, monitor SST trends and detect El Niño events.

Conflict of Interest

The authors declare that they have no conflict of interest.

Acknowledgments
The authors thank J. Hadji-Lazaro, C. Wespes for useful discussions. This work was supported by the CNES. It is based on observations with IASI embarked on Metop. The authors acknowledge the Aeris data infrastructure (https://www.aeris-data.fr/) for providing access to the IASI Level-1C data and Level-2 temperature data used in this study. This project has received funding from the European Research Council (ERC) under the European Union's Horizon 2020 and innovation program (grant agreement No 742909). L. Clarisse is Research Associate (Chercheur Qualifié) with the Belgian F.R.S.-FNRS. Ana Parracho and Simon Whitburn are grateful to the ERC for funding their research work.

Data Availability Statement

The IASI data presented in this study is available at the time of publishing this study at this website: https://iasi-ft.eu/data-access/SST/ (DOI: 10.21413/iasi-ft_metopa_sst_l3_latmos-ulb).

References

August, T., Klaes, D., Schlüssel, P., Hultberg, T., Crapeau, M., Arriaga, A., et al. (2012). IASI on Metop-A: Operational Level 2 retrievals after five years in orbit. *Journal of Quantitative Spectroscopy and Radiative Transfer*, *113*(11), 1340–1371. https://doi.org/10.1016/j.jqsrt.2012.02.028

Aumann, H. H., Chahine, M. T., & Barron, D. (2003). Sea surface temperature measurements with AIRS: RTG. SST comparison. In *Earth observing systems VIII* (Vol. *5151*, pp. 252–261). International Society for Optics and Photonics.

Barton, I. J. (1995). Satellite-derived sea surface temperatures: Current status. *Journal of Geophysical Research: Oceans*, *100*(C5), 8777–8790. https://doi.org/10.1029/95jc00365

Barton, I. J. (2011). Improving satellite-derived sea surface temperature accuracies using water vapor profile data. *Journal of Atmospheric and Oceanic Technology*, *28*(1), 85–93. https://doi.org/10.1175/2010jtecha1502.1

Belkin, I. M., Levitus, S., Antonov, J., & Malmberg, S.-A. (1998). "Great salinity anomalies" in the North Atlantic. *Progress in Oceanography*, *41*(1), 1–68. https://doi.org/10.1016/s0079-6611(98)00015-9

Bottomley, M., Folland, C. K., Hsiung, J., Newell, R. E., & Parker, D. E. (1990). *Global ocean surface temperature Atlas 'GOSTA'. A Joint Project of the Meteorological Office and the Department of Earth, Atmospheric and Planetary Sciences*. Massachusetts Institute of Technology. Metrological Office.

Bouillon, M., Safieddine, S., Hadji-Lazaro, J., Whitburn, S., Clarisse, L., Doutriaux-Boucher, M., et al. (2020). Ten-year assessment of IASI radiance and temperature. *Remote Sensing*, *12*, 2393. https://doi.org/10.3390/rs12152393

Brindley, H., Bantges, R., Russell, J., Murray, J., Dancel, C., Belotti, C., & Harries, J. (2015). Spectral signatures of earth's climate variability over 5 years from IASI. *Journal of Climate*, *28*(4), 1649–1660. https://doi.org/10.1175/jcli-d-14-00431.1

Caesar, L., Rahmstorf, S., Robinson, A., Feulner, G., & Saba, V. (2018). Observed fingerprint of a weakening Atlantic Ocean overturning circulation. *Nature*, *556*(7700), 191–196. https://doi.org/10.1038/s41586-018-0006-5

Cane, M. A., Clement, A. C., Kaplan, A., Kushnir, Y., Pozdnyakov, D., Seager, R., et al. (1997). Twentieth-century sea surface temperature trends. *Science*, *275*(5302), 957–960. https://doi.org/10.1126/science.275.5302.957

Casey, K. S., Brandon, T. B., Cornillon, P., & Evans, R. (2010). The past, present, and future of the AVHRR Pathfinder SST program. In *Oceanography from space* (pp. 273–287). Springer.

Clerbaux, C., Boynard, A., Clarisse, L., George, M., Hadji-Lazaro, J., Herbin, H., et al. (2009). Monitoring of atmospheric composition using the thermal infrared IASI/MetOp sounder. *Atmospheric Chemistry and Physics*, *9*, 6041–6054. https://doi.org/10.5194/acp-9-6041-2009

Clerbaux, C., & Crevoisier, C. (2013). New directions: Infrared remote sensing of the troposphere from satellite: Less, but better. *Atmospheric Environment*, *72*, 24–26. https://doi.org/10.1016/j.atmosenv.2013.01.057

Clerbaux, C., Hadji-Lazaro, J., Turquety, S., Mégie, G., & Coheur, P.-F. (2003). Trace gas measurements from infrared satellite for chemistry and climate applications. *Atmospheric Chemistry and Physics*, *3*, 1495–1508. https://doi.org/10.5194/acp-3-1495-2003

Collard, A. D., & McNally, A. P. (2009). The assimilation of infrared atmospheric sounding interferometer radiances at ECMWF. *Quarterly Journal of the Royal Meteorological Society*, *135*(641), 1044–1058. https://doi.org/10.1002/qj.410

Compo, G. P., & Sardeshmukh, P. D. (2010). Removing ENSO-related variations from the climate record. *Journal of Climate*, *23*(8), 1957–1978. https://doi.org/10.1175/2009jcli2735.1

Crevoisier, C., Clerbaux, C., Guidard, V., Phulpin, T., Armante, R., Barret, B., et al. (2014). Toward IASI-New Generation (IASI-NG): Impact of improved spectral resolution and radiometric noise on the retrieval of thermodynamic, chemistry and climate variables. *Atmospheric Measurement Techniques*, *7*, 4367–4385. https://doi.org/10.5194/amt-7-4367-2014

Deser, C., Phillips, A. S., & Alexander, M. A. (2010). Twentieth century tropical sea surface temperature trends revisited. *Geophysical Research Letters*, *37*(10). https://doi.org/10.1029/2010gl043321

Dickson, R. R., Meincke, J., Malmberg, S.-A., & Lee, A. J. (1988). The "great salinity anomaly" in the Northern North Atlantic 1968-1982. *Progress in Oceanography*, *20*(2), 103–151. https://doi.org/10.1016/0079-6611(88)90049-3

Dima, M., & Lohmann, G. (2010). Evidence for two distinct modes of large-scale ocean circulation changes over the last century. *Journal of Climate*, *23*(1), 5–16. https://doi.org/10.1175/2009jcli2867.1

Donlon, C., Berruti, B., Buongiorno, A., Ferreira, M.-H., Féménias, P., Frerick, J., et al. (2012). The global monitoring for environment and security (GMES) sentinel-3 mission. *Remote Sensing of Environment*, *120*, 37–57. https://doi.org/10.1016/j.rse.2011.07.024

Donlon, C. J., Minnett, P. J., Gentemann, C., Nightingale, T. J., Barton, I. J., Ward, B., & Murray, M. J. (2002). Toward improved validation of satellite sea surface skin temperature measurements for climate research. *Journal of Climate*, *15*(4), 353–369. https://doi.org/10.1175/1520-0442(2002)015<0353:tivoss>2.0.co;2

ECMWF. (2016). *IFS Documentation – Cy43r1 operational implementation 22 Nov 2016 part IV: Physical processes*.

Emery, W. J., Castro, S., Wick, G. A., Schluessel, P., & Donlon, C. (2001). Estimating sea surface temperature from infrared satellite and in situ temperature data. *Bulletin of the American Meteorological Society*, *82*(12), 2773–2785. https://doi.org/10.1175/1520-0477(2001)082<2773:esstfi>2.3.co;2

Emery, W. J., Yu, Y., Wick, G. A., Schluessel, P., & Reynolds, R. W. (1994). Correcting infrared satellite estimates of sea surface temperature for atmospheric water vapor attenuation. *Journal of Geophysical Research*, *99*(C3), 5219–5236. https://doi.org/10.1029/93jc03215

EUMETSAT. (2017a). *IASI level 1: Product guide*.

EUMETSAT. (2017b). *IASI level 2: Product guide*.

EUMETSAT. (2018). *EUMETSAT annual report 2017*.

GCOS, G. (2006). *Systematic observation requirements for satellite-based products for climate* (Vol. 1338, p. 103). WMO/TD.

Good, S. A., Embury, O., Bulgin, C. E., & Mittaz, J. (2019). *ESA sea surface temperature climate change Initiative (SST_CCI): Level 4 analysis climate data record, version 2.1*. Centre for Environmental Data Analysis. https://doi.org/10.5285/62c0f97b1eac4e0197a674870afe1ee6

Hersbach, H., Bell, B., Berrisford, P., Hirahara, S., Horányi, A., Muñoz-Sabater, J., et al. (2020). The ERA5 global reanalysis. *Quarterly Journal of the Royal Meteorological Society*, *146*(730), 1999–2049. https://doi.org/10.1002/qj.3803

Hewison, T. J., Wu, X., Yu, F., Tahara, Y., Hu, X., Kim, D., & Koenig, M. (2013). GSICS inter-calibration of infrared channels of geostationary imagers using Metop/IASI. *IEEE Transactions on Geoscience and Remote Sensing*, *51*(3), 1160–1170. https://doi.org/10.1109/tgrs.2013.2238544

Hilton, F., Armante, R., August, T., Barnet, C., Bouchard, A., Camy-Peyret, C., et al. (2012). Hyperspectral Earth observation from IASI: Five years of accomplishments. *Bulletin of the American Meteorological Society*, *93*(3), 347–370. https://doi.org/10.1175/bams-d-11-00027.1

Hirahara, S., Balmaseda, M. A., de Boisseson, E., & Hersbach, H. (2016). *26 sea surface temperature and sea ice concentration for ERA5*.

Horrocks, L. A., Candy, B., Nightingale, T. J., Saunders, R. W., O'Carroll, A., & Harris, A. R. (2003). Parameterizations of the ocean skin effect and implications for satellite-based measurement of sea-surface temperature. *Journal of Geophysical Research: Oceans*, *108*(C3). https://doi.org/10.1029/2002jc001503

Hurrell, J. W., & Trenberth, K. E. (1999). Global sea surface temperature analyses: Multiple problems and their implications for climate analysis, modeling, and reanalysis. *Bulletin of the American Meteorological Society*, *80*(12), 2661–2678. https://doi.org/10.1175/1520-0477(1999)080<2661:gsstam>2.0.co;2

Intergovernmental Panel on Climate Change. (2013). *IPCC working Group I. Climate change 2013-the physical science basis: Summary for policymakers*.

Karl, T. R., Quayle, R. G., & Groisman, P. Y. (1993). Detecting climate variations and change: New challenges for observing and data management systems. *Journal of Climate*, *6*(8), 1481–1494. https://doi.org/10.1175/1520-0442(1993)006<1481:dcvacn>2.0.co;2

Kendall, M. G. (1948). *Rank correlation methods*.

Kilpatrick, K. A., Podestá, G. P., & Evans, R. (2001). Overview of the NOAA/NASA advanced very high resolution radiometer Pathfinder algorithm for sea surface temperature and associated matchup database. *Journal of Geophysical Research*, *106*(C5), 9179–9197. https://doi.org/10.1029/1999jc000065

Konda, M., Imasato, N., Nishi, K., & Toda, T. (1994). Measurement of the sea surface emissivity. *Journal of Oceanography*, *50*(1), 17–30. https://doi.org/10.1007/bf02233853

Latif, M., & Keenlyside, N. S. (2009). El Niño/Southern Oscillation response to global warming. *Proceedings of the National Academy of Sciences*, *106*(49), 20578–20583.

Le Borgne, P., Legendre, G., & Marsouin, A. (2007). Operational SST retrieval from MetOp/AVHRR. In *Proceedings of 2007 EUMETSAT Conference*.

Lee, T., & Gentemann, C. (2018). Satellite SST and SSS observations and their roles to constrain ocean models. *New Frontiers in Operational Oceanography*, 271–288.

Li, X., Pichel, W., Maturi, E., Clemente-Colón, P., & Sapper, J. (2001). Deriving the operational nonlinear multichannel sea surface temperature algorithm coefficients for NOAA-15 AVHRR/3. *International Journal of Remote Sensing*, *22*(4), 699–704. https://doi.org/10.1080/01431160010013793

Macias, D., Garcia-Gorriz, E., & Stips, A. (2013). Understanding the causes of recent warming of Mediterranean waters. How much could be attributed to climate change? *PLoS One*, *8*(11). https://doi.org/10.1371/journal.pone.0081591

Mann, H. B. (1945). Nonparametric tests against trend. *Econometrica*, *13*, 245–259. https://doi.org/10.2307/1907187

Marsouin, A., Le Borgne, P., Legendre, G., Péré, S., & Roquet, H. (2015). Six years of OSI-SAF METOP-A AVHRR sea surface temperature. *Remote Sensing of Environment*, *159*, 288–306. https://doi.org/10.1016/j.rse.2014.12.018

Marullo, S., Artale, V., & Santoleri, R. (2011). The SST multidecadal variability in the Atlantic-Mediterranean region and its relation to AMO. *Journal of Climate*, *24*, 4385–4401. https://doi.org/10.1175/2011jcli3884.1

Masuda, K., Takashima, T., & Takayama, Y. (1988). Emissivity of pure and sea waters for the model sea surface in the infrared window regions. *Remote Sensing of Environment*, *24*(2), 313–329. https://doi.org/10.1016/0034-4257(88)90032-6

McClain, E. P., Pichel, W. G., & Walton, C. C. (1985). Comparative performance of AVHRR-based multichannel sea surface temperatures. *Journal of Geophysical Research*, *90*(C6), 11587–11601. https://doi.org/10.1029/jc090ic06p11587

McLaren, A., Fiedler, E., Roberts-Jones, J., Martin, M., Mao, C., & Good, S. (2016). *Quality information document global ocean OSTIA near real time level 4 sea surface temperature product*.

Merchant, C. J. (2013). Thermal remote sensing of sea surface temperature. In *Thermal infrared remote sensing* (pp. 287–313). Springer.

Merchant, C. J., Embury, O., Bulgin, C. E., Block, T., Corlett, G. K., Fiedler, E., et al. (2019). Satellite-based time-series of sea-surface temperature since 1981 for climate applications. *Scientific Data*, *6*, 223. http://doi.org/10.1038/s41597-019-0236-x

Merchant, C. J., & Le Borgne, P. (2004). Retrieval of sea surface temperature from space, based on modeling of infrared radiative transfer: Capabilities and limitations. *Journal of Atmospheric and Oceanic Technology*, *21*(11), 1734–1746. https://doi.org/10.1175/jtech1667.1

Merchant, C. J., Le Borgne, P., Marsouin, A., & Roquet, H. (2008). Optimal estimation of sea surface temperature from split-window observations. *Remote Sensing of Environment*, *112*(5), 2469–2484. https://doi.org/10.1016/j.rse.2007.11.011

Minnett, P. J. (1990). The regional optimization of infrared measurements of sea surface temperature from space. *Journal of Geophysical Research*, *95*(C8), 13497–13510. https://doi.org/10.1029/jc095ic08p13497

Minnett, P. J., Alvera-Azcárate, A., Chin, T. M., Corlett, G. K., Gentemann, C. L., Karagali, I., & Santoleri, R. (2019). Half a century of satellite remote sensing of sea-surface temperature. *Remote Sensing of Environment*, *233*, 111366. https://doi.org/10.1016/j.rse.2019.111366

Minnett, P. J., Evans, R. H., Kearns, E. J., & Brown, O. B. (2002). Sea-surface temperature measured by the Moderate Resolution Imaging Spectroradiometer (MODIS). In *IEEE International Geoscience and Remote Sensing Symposium* (Vol. *2*, pp. 1177–1179). IEEE.

Nalli, N. R., Minnett, P. J., & Van Delst, P. (2008). Emissivity and reflection model for calculating unpolarized isotropic water surface-leaving radiance in the infrared I: Theoretical development and calculations. *Applied Optics*, *47*(21), 3701–3721. https://doi.org/10.1364/ao.47.003701

Nykjaer, L. (2009). Mediterranean Sea surface warming 1985-2006. *Climate Research*, *39*(1), 11–17. https://doi.org/10.3354/cr00794

O'Carroll, A. G., August, T., Le Borgne, P., & Marsouin, A. (2012). The accuracy of SST retrievals from Metop-A IASI and AVHRR using the EUMETSAT OSI-SAF matchup dataset. *Remote Sensing of Environment*, *126*, 184–194. https://doi.org/10.1016/j.rse.2012.08.006

Peterson, B. J., Holmes, R. M., McClelland, J. W., Vörösmarty, C. J., Lammers, R. B., Shiklomanov, A. I., et al. (2002). Increasing river discharge to the Arctic Ocean. *Science*, *298*(5601), 2171–2173. https://doi.org/10.1126/science.1077445

Pisano, A., Marullo, S., Artale, V., Falcini, F., Yang, C., Leonelli, F. E., et al. (2020). New Evidence of Mediterranean Climate Change and Variability from Sea Surface Temperature Observations. *Remote Sensing*, *12*(1), 132. https://doi.org/10.3390/rs12010132

Qiu, B. (2000). Interannual variability of the Kuroshio Extension system and its impact on the wintertime SST field. *Journal of Physical Oceanography*, *30*(6), 1486–1502. https://doi.org/10.1175/1520-0485(2000)030<1486:ivotke>2.0.co;2

Rahmstorf, S., Box, J. E., Feulner, G., Mann, M. E., Robinson, A., Rutherford, S., & Schaffernicht, E. J. (2015). Exceptional twentieth-century slowdown in Atlantic Ocean overturning circulation. *Nature Climate Change*, *5*(5), 475. https://doi.org/10.1038/nclimate2554

Rayner, N. A., Kaplan, A., Kent, E. C., Reynolds, R. W., Brohan, P., Casey, K. S., et al. (2009). Evaluating climate variability and change from modern and historical SST observations. In *Proceedings of OceanObs' 09: Sustained ocean observations and information for society* (*2*).

Rayner, N. A., Parker, D. E., Horton, E. B., Folland, C. K., Alexander, L. V., Rowell, D. P., et al. (2003). Global analyses of sea surface temperature, sea ice, and night marine air temperature since the late nineteenth century. *Journal of Geophysical Research: Atmospheres*, *108*(D14). https://doi.org/10.1029/2002jd002670

Reynolds, R. W., Rayner, N. A., Smith, T. M., Stokes, D. C., & Wang, W. (2002). An improved in situ and satellite SST analysis for climate. *Journal of Climate*, *15*(13), 1609–1625. https://doi.org/10.1175/1520-0442(2002)015<1609:aiisas>2.0.co;2

Robinson, I., Piollé, J.-F., LeBorgne, P., Poulter, D., Donlon, C., & Arino, O. (2012). Widening the application of AATSR SST data to operational tasks through the Medspiration Service. *Remote Sensing of Environment*, *116*, 126–139. https://doi.org/10.1016/j.rse.2010.12.019

Robinson, I. S. (2004). *Measuring the oceans from space: The principles and methods of satellite oceanography*. Springer Science & Business Media.

Robinson, I. S., & Donlon, C. J. (2003). Global measurement of sea surface temperature from space: Some new perspectives. *The Global Atmosphere and Ocean System*, *9*(1–2), 19–37. https://doi.org/10.1080/1023673031000080385

Saunders, R., Hocking, J., Rundle, D., Rayer, P., Hayemann, S., Matricardi, M., et al. (2017). *RTTOV-12 science and validation report* (EUMETSAT NWP SAF report NWPSAF-MO-TV-41).

Saunders, R., Hocking, J., Turner, E., Rayer, P., Rundle, D., Brunel, P., et al. (2018). An update on the RTTOV fast radiative transfer model (currently at version 12). *Geoscientific Model Development*, *11*(7). https://doi.org/10.5194/gmd-11-2717-2018

Sen, P. K. (1968). Estimates of the regression coefficient based on Kendall's tau. *Journal of the American Statistical Association*, *63*(324), 1379–1389. https://doi.org/10.1080/01621459.1968.10480934

Siméoni, D., Singer, C., & Chalon, G. (1997). Infrared atmospheric sounding interferometer. *Acta Astronautica*, *40*(2–8), 113–118. https://doi.org/10.1016/s0094-5765(97)00098-2

Smith, N., Smith, W. L., Weisz, E., & Revercomb, H. E. (2015). AIRS, IASI, and CrIS retrieval records at climate scales: An investigation into the propagation of systematic uncertainty. *Journal of Applied Meteorology and Climatology*, *54*(7), 1465–1481. https://doi.org/10.1175/jamc-d-14-0299.1

Ssenyunzi, R. C., Oruru, B., D'ujanga, F. M., Realini, E., Barindelli, S., Tagliaferro, G., et al. (2020). Performance of ERA5 data in retrieving Precipitable Water Vapor over East African tropical region. *Advances in Space Research*, *65*(8), 1877–1893. https://doi.org/10.1016/j.asr.2020.02.003

Theil, H. (1992). A rank-invariant method of linear and polynomial regression analysis. In *Henri Theil's contributions to economics and econometrics* (pp. 345–381). Springer.

Van Damme, M., Whitburn, S., Clarisse, L., Clerbaux, C., Hurtmans, D., & Coheur, P. F. (2017). *Version 2 of the IASI NH 3 neural network retrieval algorithm: Near-real-time and reanalyzed datasets*.

Vargas-Yáñez, M., García, M. J., Salat, J., García-Martínez, M. C., Pascual, J., & Moya, F. (2008). Warming trends and decadal variability in the Western Mediterranean shelf. *Global and Planetary Change*, *63*(2–3), 177–184. https://doi.org/10.1016/j.gloplacha.2007.09.001

Vecchi, G. A., Clement, A., & Soden, B. J. (2008). Pacific signature of global warming: El Nino or La Nina. *Eos, Transactions American Geophysical Union*, *89*(9). https://doi.org/10.1029/2008eo090002

Walton, C. C., Pichel, W. G., Sapper, J. F., & May, D. A. (1998). The development and operational application of nonlinear algorithms for the measurement of sea surface temperatures with the NOAA polar-orbiting environmental satellites. *Journal of Geophysical Research*, *103*(C12), 27999–28012. https://doi.org/10.1029/98jc02370

Wills, S. M., Thompson, D. W. J., & Ciasto, L. M. (2016). On the observed relationships between variability in Gulf Stream sea surface temperatures and the atmospheric circulation over the North Atlantic. *Journal of Climate*, *29*(10), 3719–3730. https://doi.org/10.1175/jcli-d-15-0820.1

Wu, X., & Smith, W. L. (1997). Emissivity of rough sea surface for 8-13 μm: Modeling and verification. *Applied Optics*, *36*(12), 2609–2619. https://doi.org/10.1364/ao.36.002609